

# Energy loss effects on heavy quark production in heavy-ion collisions at $\sqrt{s} = 5.5 \text{ ATeV}^*$

Ziwei Lin<sup>a</sup> and Ramona Vogt<sup>a,b</sup>

<sup>a</sup>Nuclear Science Division, LBNL, Berkeley, CA 94720

<sup>b</sup>Physics Department, University of California at Davis, Davis, CA 95616

## Abstract

We study the effect of energy loss on charm and bottom quarks in high-energy heavy-ion collisions including hadronization, longitudinal expansion and partial thermalization. We consider in detail the detector geometry and single lepton energy cuts of the ALICE and CMS detectors at the Large Hadron Collider (LHC) to show the large suppression of high  $p_T$  heavy quarks and the consequences of their semileptonic decays.

Typeset using REVTeX

---

\*This work was supported in part by the Director, Office of Energy Research, Division of Nuclear Physics of the Office of High Energy and Nuclear Physics of the U. S. Department of Energy under Contract Number DE-AC03-76SF00098.

## I. INTRODUCTION

A dense parton system is expected to be formed in the early stage of relativistic heavy-ion collisions due to the onset of hard and semihard parton scatterings. Interactions among the produced partons in this dense medium will most likely lead to partial thermalization and formation of a quark-gluon plasma. It is thus important to study phenomenological signals of the early parton dynamics, a crucial step towards establishing the existence of a strongly interacting initial system and its approach to thermal equilibrium.

The energy loss of fast partons is a good probe of dense matter [1] since a fast parton traversing the medium must experience multiple elastic collisions [2,3] as well as suffer radiative energy loss [4–7]. In principle, the energy loss by a parton in medium, both by elastic [2,3] and radiative [4–7] processes, is independent of the quark mass in the infinite energy limit. At finite energies, studies show that the elastic energy loss has a weak mass dependence. For example, in a medium with  $\alpha_s = 0.3$ ,  $n_f \approx 2.5$  and a temperature of 500 MeV, the elastic  $dE/dx$  for 10 GeV charm and bottom quarks is  $\approx -1.5$  and  $-0.5$  GeV/fm, respectively [7]. The radiative loss is perhaps even more important. Taking into account multiple scatterings and the Landau-Pomeranchuk-Midgal effect, the radiative energy loss of a fast massless quark,  $dE/dx \simeq -3\alpha_s \langle p_{T_w}^2 \rangle / 8$  [6], is controlled by the characteristic broadening of the transverse momentum squared of the parton,  $\langle p_{T_w}^2 \rangle$ , determined by the properties of the medium. Recent estimates of the radiative loss by charm and bottom quarks [7] suggest that the loss from this source is much greater than the elastic loss,  $dE/dx = -7.5$  and  $-5$  GeV/fm for 10 GeV charm and bottom quarks respectively. The calculated loss depends on the initial energy of the parton and the density of the medium. It is also unclear precisely where these analytical results are applicable. In this paper, we will assume a constant loss of  $dE/dx = -1$  GeV/fm to study the phenomenology of energy loss on heavy quarks at the LHC.

Since heavy-flavored mesons carry most of the heavy quark energy after hadronization, the energy lost by heavy quarks traveling through the quark-gluon plasma is directly reflected

in the suppression of large  $p_T$  heavy-flavored mesons.

Unfortunately, it is difficult to detect charm or bottom mesons directly with current tracking technology because of the large number of produced particles in central  $AA$  collisions. However, the invariant mass of the lepton pairs from heavy quark decays is related to the relative momentum of the  $Q\bar{Q}$  pair, the dilepton yields in this region could become an indirect measurement of the heavy quark spectrum. Therefore, it should be sensitive to the energy loss suffered by the heavy quarks as they propagate through dense matter.

In this paper, we examine the effects of heavy quark energy loss at LHC energies,  $\sqrt{s} = 5.5$  TeV for Pb+Pb collisions, including hadronization of the heavy quarks, longitudinal expansion and thermal fluctuations of the collision system, which are important for the dilepton spectrum from heavy quark decays. At the LHC energy, the heavy quarks are produced at sufficiently large  $p_T$  for the hadronization mechanism to be important. Because of the longitudinal expansion, the momentum loss in the longitudinal direction is quite different from that in the transverse direction. Depending on the actual number of scatterings, the heavy quarks can escape the system without energy loss or lose enough momentum to be stopped entirely. However, heavy quarks cannot be at rest in a thermal environment. In the most extreme scenario when they are stopped, they must have a thermal momentum distribution in their local frame. The resulting suppression of high invariant mass dileptons is then very sensitive to the phase space restrictions imposed by the detector design.

This paper is organized as follows. We explain our energy loss model in section II. In section III, we discuss the effects of energy loss on the charm and bottom quark spectra and show the resulting dilepton spectra from correlated heavy meson decays. To demonstrate the sensitivity to the phase space restriction, in section IV we calculate the spectra of  $e^+e^-$ ,  $e^\pm\mu^\mp$  and  $\mu^+\mu^-$  pairs from correlated heavy meson pair decays within the planned acceptances of the ALICE detector, taking into account the detector geometry and single lepton energy cuts. The  $\mu^+\mu^-$  spectra within the CMS geometry is also calculated. In section V we calculate the single  $e$  and  $\mu$  spectra from charm and bottom decays within the ALICE and CMS acceptances. We summarize in section VI.

## II. MODELING THE ENERGY LOSS

First, the phase space distribution of the heavy quarks and the space-time evolution of the dense matter must be specified. In the Bjorken model [8], the matter has a longitudinal fluid velocity  $v_z^F = z/t$  in the local frame, essentially the fluid velocity of free-streaming particles produced at  $z = 0$  and  $t = 0$ . Transverse flow, which sets in later, is neglected and both the medium and the heavy quarks are assumed to be produced at  $z = 0$ , the same point at which expansion begins. Then, for any space-time point,  $(z, t)$ , a heavy quark is in a fluid with the same longitudinal velocity. In the fluid rest frame, the heavy quark thus has momentum  $(0, \vec{p}_T)$ , reduced to  $(0, \vec{p}_T')$  after energy loss. Thus the momentum of the heavy quark changes from  $(m_T \sinh y, \vec{p}_T)$  to  $(m_T' \sinh y, \vec{p}_T')$  in the lab frame. The heavy quark essentially loses its transverse momentum but retains its rapidity because it follows the longitudinal flow.

To simplify the calculations, spherical nuclei of radius  $R_A = 1.2A^{1/3}$  are assumed so that the transverse area of the system in central collisions is the area of the nucleus, neglecting transverse expansion. For a heavy quark with a transverse path,  $l_T$ , and mean-free path,  $\lambda$ , in the medium, the average number of scatterings is  $\mu = l_T/\lambda$ . The mean-free path is introduced to account for the finite probability of the heavy quarks to escape the system without interaction or energy loss. The actual number of scatterings,  $n$ , is generated from the Poisson distribution,  $P(n, \mu) = e^{-\mu} \mu^n / n!$ . This corona effect is especially important for heavy quarks produced at the edge of the transverse plane of the collision. In the rest frame of the medium, the heavy quark then experiences a total momentum loss of  $\Delta p = n\lambda dE/dx$ .

When a heavy quark loses most or all of its momentum in the fluid rest frame, it begins to thermalize with the dense medium. The heavy quark is considered to be thermalized if its final transverse momentum after energy loss,  $p_T'$ , is smaller than the average transverse momentum of thermalized heavy quarks at temperature  $T$ . These thermalized heavy quarks have a random thermal momentum in the rest frame of the fluid. The final momentum of the thermalized heavy quark is obtained by transforming back from the local fluid frame

to the center-of-mass frame of the collision. The parameters used in the calculation are  $dE/dx = -1$  GeV/fm,  $\lambda = 1$  fm and  $T = 150$  MeV. Simulations at RHIC energies [9] suggest that once the heavy quarks are assumed to lose energy, significant suppression of the heavy quark spectra appears as long as  $|dE/dx| \geq \langle p_T \rangle / R_A$  where  $\langle p_T \rangle$  is the average transverse momentum of the heavy quark which produces leptons inside the detector acceptance. *E.g.* at central rapidities with Pb beams and  $\langle p_T \rangle = 3$  GeV, the threshold energy loss is as low as  $\langle p_T \rangle / R_A \sim 0.4$  GeV/fm.

### III. EFFECTS OF ENERGY LOSS ON HEAVY QUARK PRODUCTION AND DECAY

The momentum distribution of the  $Q\bar{Q}$  pairs is generated from PYTHIA 6.115 [10]. Initial and final state radiation effectively simulates higher-order contributions to heavy quark production so that the pair is no longer azimuthally back-to-back as at leading order. The MRS D- $'$  [11] parton distribution functions are used to normalize the charm pair production cross section to 17.7 mb in  $pp$  collisions at  $\sqrt{s} = 5.5$  GeV [12]. The number of  $Q\bar{Q}$  pairs in a Pb+Pb collision at impact parameter  $b = 0$  is obtained by multiplying the  $pp$  production cross section by the nuclear overlap function,

$$N_{Q\bar{Q}} = \sigma_{Q\bar{Q}}^{pp} T_{\text{PbPb}}(\mathbf{0}) \quad (1)$$

where  $T_{\text{PbPb}}(\mathbf{0}) = 30.4/\text{mb}$ . This scaling results in 540 charm pairs in a central Pb+Pb event. The  $b\bar{b}$  production cross section is 224  $\mu\text{b}$  in  $\sqrt{s} = 5.5$  TeV  $pp$  collisions, leading to 6.8  $b\bar{b}$  pairs in central Pb+Pb events. Although, as pointed out in the introduction, the bottom quark energy loss may be different from that of charm quarks, the same parameters are used.

Only dileptons from correlated  $Q\bar{Q}$  pair decays,  $N_{ll}^{\text{corr}} = N_{Q\bar{Q}} B^2(Q/\bar{Q} \rightarrow l^\pm X)$  are considered, *i.e.*, a single  $Q\bar{Q}$  pair produces the dilepton. Dileptons from uncorrelated  $Q\bar{Q}$  decays, which appear at higher invariant mass than those from correlated decays

due to their larger rapidity gap, will be particularly abundant for charm decays since  $N_l^{\text{uncorr}} = N_{Q\bar{Q}}(N_{Q\bar{Q}} - 1)B^2(Q/\bar{Q} \rightarrow l^\pm X)$ . The finite acceptance of a real detector will significantly reduce the uncorrelated rate and like-sign subtraction should remove most of the remainder. In practice however, full subtraction will be difficult. Another problem arises from uncorrelated lepton pairs from a heavy quark and a background  $\pi$  or  $K$  decay. Treatment of these uncorrelated backgrounds is not considered in this work.

Since the dilepton spectra in the LHC detectors are sensitive to decays of charm quarks with  $p_T > 20$  GeV, the charm spectrum was generated in two steps to obtain a sufficient number of high  $p_T$  charm quarks. First  $10^5$  normal  $c\bar{c}$  pairs were generated followed by an equal number of  $c\bar{c}$  pairs with a high  $p_T$  trigger such that the  $c\bar{c}$  pair spectrum contains pairs with  $p_{T,c} > 5$  GeV and  $p_{T,\bar{c}} > 5$  GeV only. These high  $p_T$   $c\bar{c}$  pairs were then removed from the normal spectrum so that the resulting soft  $c\bar{c}$  spectrum contains those pairs with  $p_{T,c} < 5$  GeV or  $p_{T,\bar{c}} < 5$  GeV. The relative weight of the high  $p_T$  spectrum is obtained from the ratio of the high  $p_T$  events to the total spectrum. Because the bottom quarks have a harder  $p_T$  spectrum than the charm quarks, such a procedure was unnecessary for  $b\bar{b}$  pairs.

In Fig. 1 the single  $D$  meson  $p_T$  distribution is shown without any phase space cuts. The spectra in Fig. 1 are normalized, as are all the figures, to a single Pb+Pb event. The dashed curve shows the generated spectra without energy loss while the solid curve is the distribution after energy loss. Thermalization of charm quarks that have lost most of their momentum causes the build-up at low  $p_T$ . At higher values of  $p_T$ , some quarks are sufficiently energetic to escape the dense medium without being thermalized. For  $p_T \geq 5$  GeV, the energy loss causes the  $p_T$  distribution to drop nearly an order of magnitude.

Figure 2 shows the corresponding single bottom  $p_T$  distribution. The same trends are seen for bottom as in Fig. 2 except that the energy loss results in only a factor of five reduction in the high  $p_T$  bottom yield.

In order to obtain the final meson distributions, the heavy quark distributions are convoluted with a fragmentation function. While a delta-function type of fragmentation is sufficient for low  $p_T$  hadroproduction [13,14], high  $p_T$  heavy quarks should fragment accord-

ing to a Peterson-type function [15],  $D(z) \propto [z(1 - 1/z - \epsilon/(1 - z))]^{-1}$  where  $z = p_H/p_Q$  and  $\epsilon = 0.06$  for charm and 0.006 for bottom, determined from  $e^+e^-$  interactions [16]. Note that the heavy quark quantities are denoted by  $Q$  while the heavy hadron formed from the fragmentation of the quark is denoted with  $H$ . A corresponding intrinsic  $k_T$  kick of 1 GeV for the partons in the proton is also included. Because fragmentation reduces the momentum of the heavy-flavored hadron relative to the heavy quark, especially for charm, the rapidity distribution of the final-state hadron is modified relative to the fluid so that the hadron does not precisely follow the longitudinal flow. In a high-energy collision,  $\sqrt{s}/m \gg 1$ , the heavy quark rapidity distribution is essentially flat. However, the hadronization of the heavy quark enhances the rapidity distribution at central rapidities. If the delta-function type of fragmentation is assumed, the momentum does not change,  $p_Q = p_H$ , but  $E_Q^2 = E_H^2 - m_H^2 + m_Q^2$ , resulting in a rapidity shift

$$dn \propto dy_Q = \frac{dp_{zQ}}{E_Q} = \frac{dp_{zH}}{E_Q} = \frac{m_{T,H} \cosh y_H dy_H}{\sqrt{m_{T,H}^2 \cosh^2 y_H - m_H^2 + m_Q^2}} \approx \frac{\cosh y_H dy_H}{\sqrt{\cosh^2 y_H - \alpha^2}} \quad (2)$$

where

$$\alpha^2 = \frac{m_H^2 - m_Q^2}{m_{T,H}^2}. \quad (3)$$

For  $m_c = 1.3$  GeV,  $m_D = 1.87$  GeV and  $m_{T,D} \approx \sqrt{2}m_D$ ,  $\alpha^2 = 0.25$ , enhancing the  $D$  distribution at  $y_H = 0$  by  $\approx 15\%$ . When  $m_b = 4.75$  GeV,  $m_B = 5.27$  GeV and  $m_{T,B} = \sqrt{2}m_B$ ,  $\alpha^2 = 0.09$ , enhancing the  $B$  distribution by  $\approx 5\%$ . The range of the enhancement is  $|y_H| < 2.5$ . If the Peterson function is used instead,  $\alpha^2$  increases,

$$\alpha^2 = \frac{m_H^2 - z^2 m_Q^2}{m_{T,H}^2}, \quad (4)$$

increasing the  $D$  enhancement at  $y_H = 0$  to  $\approx 30\%$  for  $\langle z \rangle \approx 0.7$  and the  $B$  enhancement to  $\approx 15\%$  for  $\langle z \rangle \approx 0.85$ . These  $\langle z \rangle$  values are typical for the Peterson function with  $\epsilon$  values given above. The fragmentation thus tends to pile-up heavy hadrons at central rapidities.

The dilepton spectrum from semileptonic charm and bottom decays may be used to indirectly measure heavy quark production when a direct measurement via tracking is difficult.

Measurements of high-mass dileptons are themselves important. Copious thermal dilepton production [17] was proposed as a signal of the formation of a thermally and chemically equilibrated quark-gluon plasma. In order to obtain the thermal dilepton yields, the background from heavy quark decays must be subtracted. When energy loss was not included, dileptons from open charm decays at RHIC were shown to be about an order of magnitude higher than the contributions from the Drell-Yan process and bottom decays [12,18], making them the dominant background to the proposed thermal dileptons. This background was determined to be even higher at the LHC [12]. Energy loss changes the heavy quark momentum distribution as well as the resulting dilepton spectra from heavy quark decays. Therefore, understanding the effect of energy loss on dileptons from heavy quark decays could also be an important step towards the observation of thermal dilepton signals.

The average branching ratios of  $\overline{D} \rightarrow lX$  are  $\approx 12\%$ . The lepton energy spectrum from  $D$  meson semileptonic decays in PYTHIA 6.115 is consistent with the measurement of the MARK-III collaboration [19]. The  $b$  quarks are assumed to fragment into  $B^-, \overline{B}^0, \overline{B}_s^0$  and  $\Lambda_b^0$  with production percentages 38%, 38%, 11% and 13%, respectively. Single leptons from bottom decays can be categorized as primary and secondary leptons. Leptons directly produced in the decay  $B \rightarrow lX$  are primary leptons while those indirectly produced,  $B \rightarrow DX \rightarrow lY$ , are secondary. Primary leptons have a harder energy spectrum than secondary leptons. A decaying  $b$  hadron mainly produces primary  $l^-$  and secondary  $l^+$  although it can also produce a smaller number of primary  $l^+$  due to  $B^0 - \overline{B}^0$  mixing. The branching ratios of the necessary bottom hadron decays are 9.30% to primary  $l^-$ , 2.07% to secondary  $l^-$ , 1.25% to primary  $l^+$ , and 7.36% to secondary  $l^+$ . The total number of dileptons from a  $b\overline{b}$  decay can be readily estimated to be 0.020. Another important source of dileptons from bottom decays is the decay of a single bottom,  $B \rightarrow Dl_1X \rightarrow l_1l_2Y$ . The branching ratio for a single  $B$  meson to a dilepton is 0.906%, therefore this source gives 0.018 dileptons, comparable to the yield from a  $b\overline{b}$  pair decay. These branching ratios [20] and energy spectra from PYTHIA 6.115, consistent with measurements [21], are almost identical for muons and electrons.

The dilepton invariant mass and rapidity are defined as:



$$\begin{aligned}
M &= \sqrt{(p_{l+}^y + p_{l-}^y)^2} \\
y &= \tanh^{-1} \frac{p_{l+}^z + p_{l-}^z}{E_{l+} + E_{l-}} .
\end{aligned}
\tag{5}$$

In Fig. 3 the dilepton invariant mass spectrum from correlated  $D\bar{D}$  decays are shown without any phase space cuts. The dashed curves are the generated spectra without energy loss while the solid curves are the distributions after energy loss. Except for the small difference between the electron and muon masses, this spectrum represents both dielectrons and dimuons while the spectrum of opposite-sign  $e\mu$  is a factor of two larger ( $e^+\mu^- + e^-\mu^+$ ).

Figure 4 shows the integrated invariant mass spectra from correlated  $B\bar{B}$  and single  $B$  decays. The dotted curve is the result of the decays of a single  $B$  to lepton pairs. When  $M < 3$  GeV, this contribution is larger than the dilepton yield from  $B\bar{B}$  decays, shown in the dot-dashed curve. Both include energy loss. The solid curve is the sum of the two contributions while the dashed curve is the sum of single and pair decays to dileptons without energy loss. The same trends are seen for bottom as well as charm except that the suppression of the spectrum due to energy loss begins at larger invariant mass. The mass distribution in Fig. 4 is truncated to more clearly show the contribution from single  $B$  decay.

In Fig. 5, the lepton pair rapidity distribution from correlated  $D\bar{D}$  decays with and without energy loss is shown. The spectrum reflects the effect of the hadronization shown in eqs. (2)-(4).

The lepton pair rapidity distribution from  $B\bar{B}$  and single  $B$  decays shows a similar shift in Fig. 6. Since the  $B\bar{B}$  decay distribution is not as broad as the  $D\bar{D}$  distribution due to the higher mass  $B\bar{B}$  pairs, the narrowing of the central peak seen in Fig. 6 is not as dramatic as the charm hadron decays in Fig. 5.

A comparison of the dilepton spectra before and after energy loss would naively suggest that the overall effect is small. However, this impression is misleading because the spectrum is integrated over the entire phase space. Heavy quarks and antiquarks in a pair tend to be separated by a significant rapidity gap. This gap can cause the invariant mass of the subsequent lepton pair to be large. However, once the finite detector geometries are included,

the effect of energy loss becomes more dramatic as we show in the following section.

## IV. DILEPTONS FROM HEAVY QUARK DECAYS IN REAL DETECTORS

### A. ALICE

The ALICE detector [22] consists of a central barrel with electron detection capability and a forward muon arm. Thus it is well suited to carry out a comparative study of single lepton ( $e, \mu$ ) and dilepton ( $ee, e\mu, \mu\mu$ ) yields comparable to the electromagnetic capabilities of the PHENIX detector [23] at RHIC. (Note that PHENIX has two muon arms.) In this section, we calculate the dilepton yields within the designed ALICE acceptance.

The ALICE central barrel covers  $\pm 45^\circ$ , corresponding to  $|\eta| < 0.9$ , with full azimuthal acceptance. The forward muon arm covers the polar angle  $2^\circ \leq \theta_\mu \leq 10^\circ$ , corresponding to the pseudo-rapidity interval  $2.5 \leq \eta_\mu \leq 4$ , again with full azimuthal coverage. We take  $p_{T,e} > 1$  GeV and  $p_{T,\mu} > 1$  GeV to reduce the lepton backgrounds from random hadron decays.

Fig. 7 shows the invariant mass distribution of three types of dileptons from open charm and bottom hadron decays within the ALICE acceptance. The  $e\mu$  spectrum includes both  $e^+\mu^-$  and  $e^-\mu^+$ . From the comparison of our energy loss results with the initial distributions, we note that the three dilepton yields from charm decays and also for bottom decays have rather similar suppression factors. This is different from the effect expected at RHIC because we use the same  $p_T$  cut for electrons and muons in ALICE while the electron and muon energy cuts are the same in PHENIX [23]. Note the similarity of the charm and bottom hadron decay rates without energy loss for  $M < 5$  GeV despite the much larger  $c\bar{c}$  production rate. Although there is significant suppression due to energy loss at high invariant mass, the peaks of the bottom decay spectra are not strongly suppressed.

To demonstrate the acceptance of the ALICE detector, in Fig. 8 we show the rapidity distribution of the three types of dileptons from charm meson decays. The  $ee$  pairs are

centered around  $y \sim 0$ , while the  $e\mu$  acceptance covers pair rapidity around 1 to 2.5 and the  $\mu\mu$  pairs are found with  $y \sim 2.5$  to 4.

We also plot the Drell-Yan yields of dielectrons and dimuons in Fig. 7. After energy loss, the Drell-Yan dileptons are greater than the open charm meson decays above 5 GeV in the  $ee$  channel and everywhere in the  $\mu\mu$  channel. However, the effect of energy loss in the model is sufficiently weak for the  $B\bar{B}$  and single  $B$  decays to remain above the Drell-Yan rate. While thermal dileptons remain essentially unobservable at the LHC, the suppression of dileptons from bottom hadron decays is similar enough to present a good opportunity to measure the energy loss. Also note that high-mass  $e\mu$  pairs cannot be used for charm measurements but for bottom observation.

## B. CMS

The CMS [24] muon acceptance is in the range  $|\eta| \leq 2.4$  with a lepton  $p_T$  cut of 3 GeV. After these simple cuts are applied, the results are shown in Fig. 9 for both  $D\bar{D}$  and  $B\bar{B}$  decays. Whereas for  $M \leq 15$  GeV, the  $D\bar{D}$  decays would dominate those of  $B\bar{B}$  before the cuts, the measured  $B\bar{B}$  decays are everywhere larger than those from charm mesons both before and after energy loss. The generally larger momentum of muons from  $B$  decays and the rather high momentum cut result in larger acceptance for  $B\bar{B}$  decays. No  $D\bar{D}$  decay pairs with  $M \leq 5$  GeV survive the momentum cut. A factor of 50 loss in rate at  $M \sim 10$  GeV is found before energy loss when comparing Figs. 9 and 3. A loss in rate by a factor of 100 is obtained when energy loss is included. The corresponding acceptance from  $B\bar{B}$  decays is significantly larger, with a loss in rate of a factor of  $\approx 8$  before energy loss and  $\approx 15$  with energy loss. Interestingly, the leptons in the decay chain of a single  $B$  meson are energetic enough for both to pass the momentum cut, causing the peak at  $M \sim 2 - 3$  GeV. These results suggest that rather than providing an indirect measurement of the charm cross section, as postulated in [12], the dilepton continuum above the  $\Upsilon$  family could instead measure the  $b\bar{b}$  production cross section indirectly. A comparison with the spectrum from

$pp$  interactions at the same energy would then suggest the amount of energy loss,  $dE/dx$ , of the medium.

To demonstrate the CMS acceptance, in Fig. 10 we show the rapidity distribution of dimuons from charm meson decays before and after energy loss. The broader rapidity coverage of CMS reduces the effect of energy loss on the dimuon continuum relative to ALICE.

## V. SINGLE LEPTONS FROM HEAVY QUARK DECAYS

Single leptons from charm decay have been suggested as an indirect measure of the charm production cross section [25]. This is possible if the background leptons from random decays of hadrons such as pions and kaons can be well understood.

We show the effect of energy loss on single electrons and muons within the ALICE acceptance in Fig. 11. Single leptons are not as sensitive to the magnitude of  $dE/dx$  as the dilepton mass spectra.

Single leptons can be categorized as those from thermalized heavy quarks and those from heavy quarks energetic enough to escape after energy loss. The former mainly reflects the effective thermalization temperature while the latter can provide us with information on the energy loss. Single leptons with energies greater than 1 – 2 GeV are mainly from energetic heavy quarks and thus are more sensitive to the energy loss. Before energy loss, the single leptons from  $D$  decays are larger than those from  $b$  hadron decays for  $p_T < 2.5$  GeV. After energy loss, the  $b$  hadron decays dominate the spectra over all  $p_T$ .

A comparison of the  $p_T$  distributions of single muons in the CMS acceptance from the decays of  $D$  and  $B$  mesons can also provide a measure of the  $b$  cross section, shown in Fig. 12. The muon  $p_T$  distribution is clearly dominated by  $B$  decays.

## VI. SUMMARY AND DISCUSSION

Dileptons from open charm and bottom decays have been calculated for central Pb+Pb collisions at the LHC including the effect of energy loss on heavy quarks in dense matter.

There are a number of uncertainties in the model. The energy loss is assumed to be constant during the expansion of the system and the subsequent drop in the energy density. This need not necessarily be the case. Transverse flow, which could lead to a higher effective temperature,  $T$ , and thus enhance the low  $p_T$  heavy quark yield and, consequently, the low invariant mass dilepton yields, is also not included. However, the qualitative features of the results, such as the clear dominance of  $b\bar{b}$  decays and the strong suppression due to energy loss when  $|dE/dx| \geq \langle p_T \rangle / R_A$ , are not likely to change.

To determine whether single leptons or dileptons from heavy quark decays can indeed probe the energy loss, the most important factor is the magnitude of the random hadron decay background. This deserves further study, particularly since high  $p_T$  pions will also experience quenching effects and be suppressed in high-energy heavy-ion collisions.

Acknowledgments: We thank M. Bedjidian, D. Denegri and A. Morsch for helpful discussions about the ALICE and CMS detectors.

FIGURES

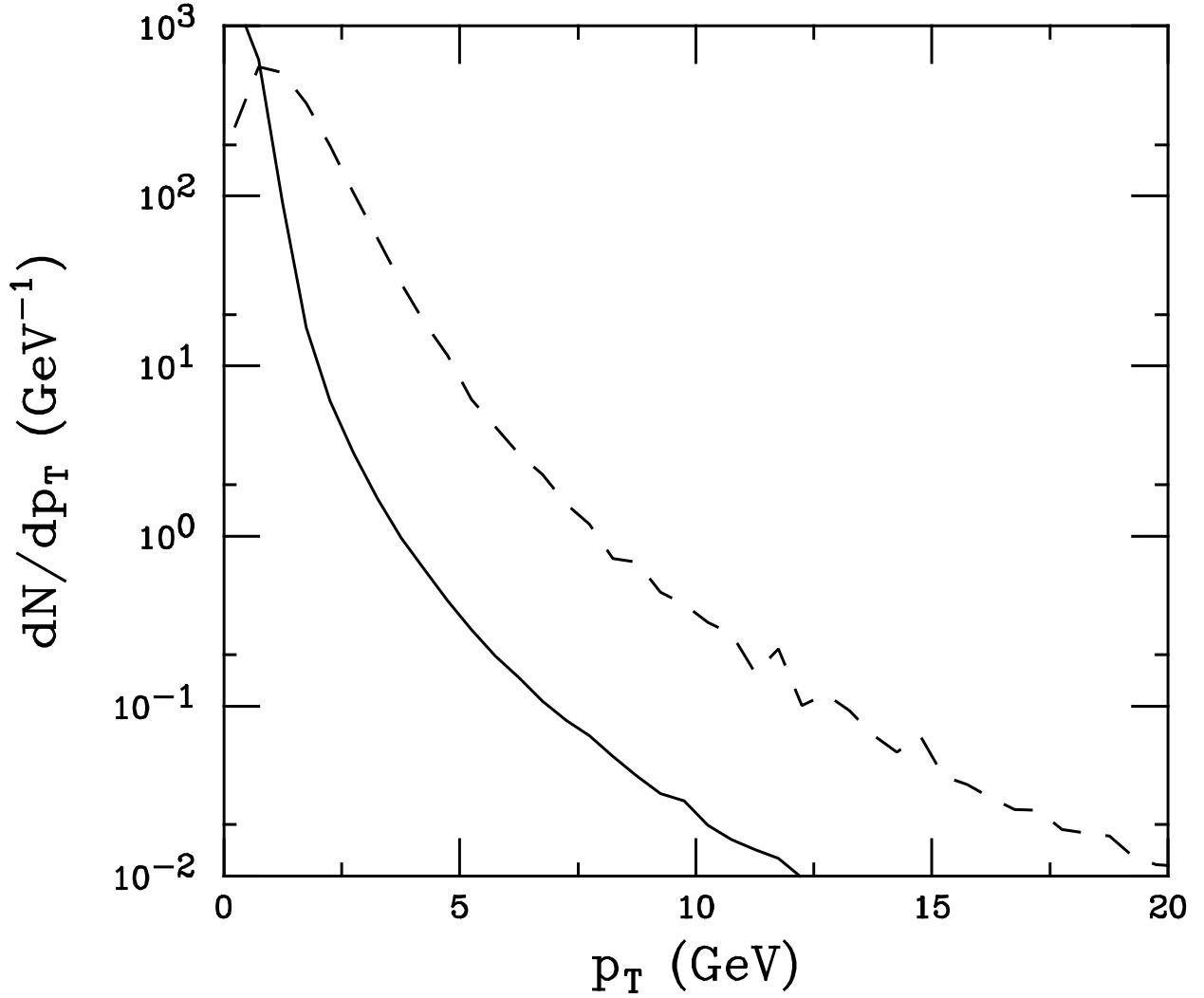


FIG. 1. The  $p_T$  distribution of single  $D$  mesons, integrated over all phase space. The dashed curve is without energy loss, the solid curve includes energy loss with  $dE/dx = -1 \text{ GeV/fm}$ .

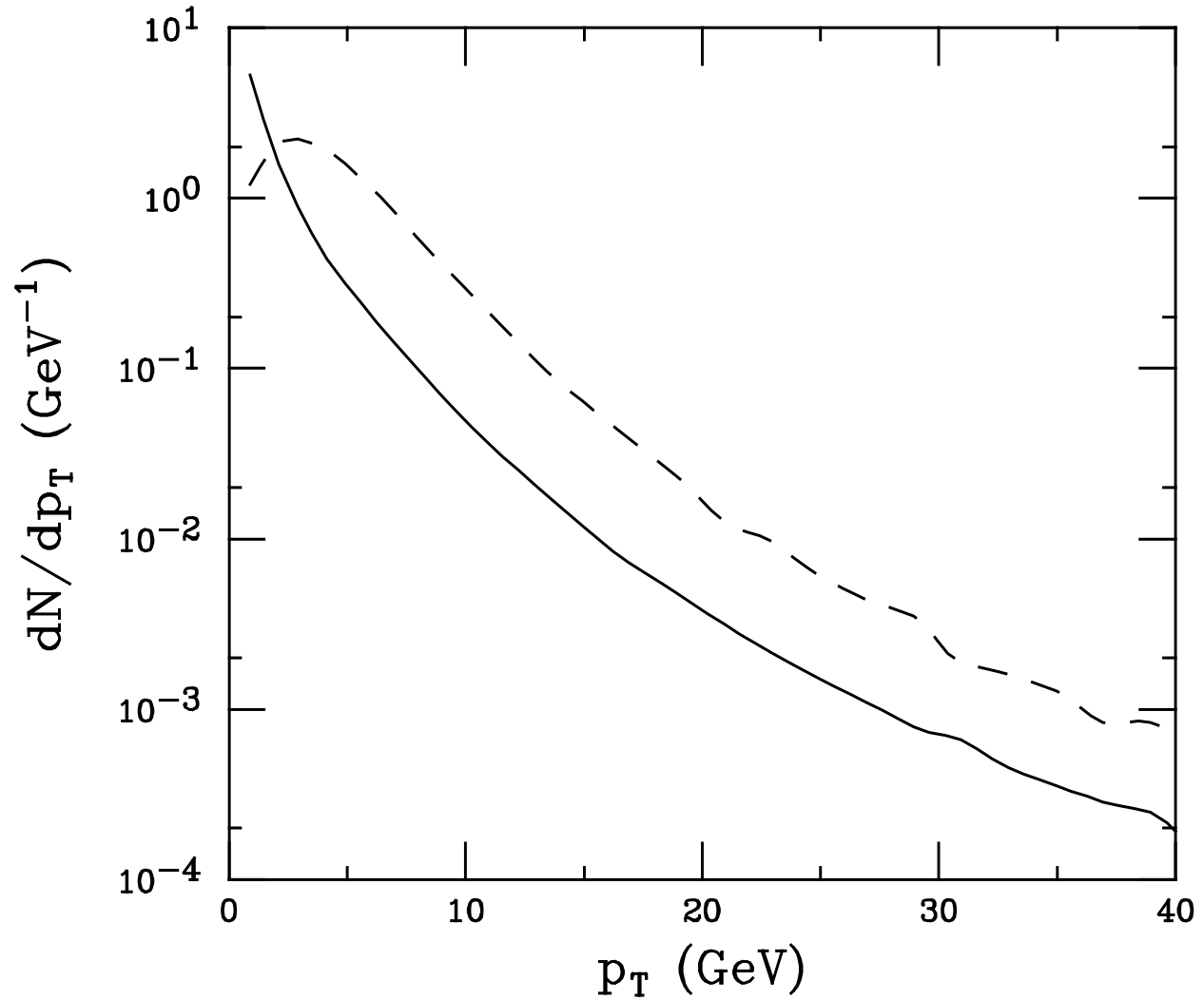


FIG. 2. The  $p_T$  distribution of single  $B$  mesons, integrated over all phase space. The dashed curve is without energy loss, the solid curve includes energy loss with  $dE/dx = -1 \text{ GeV/fm}$ .

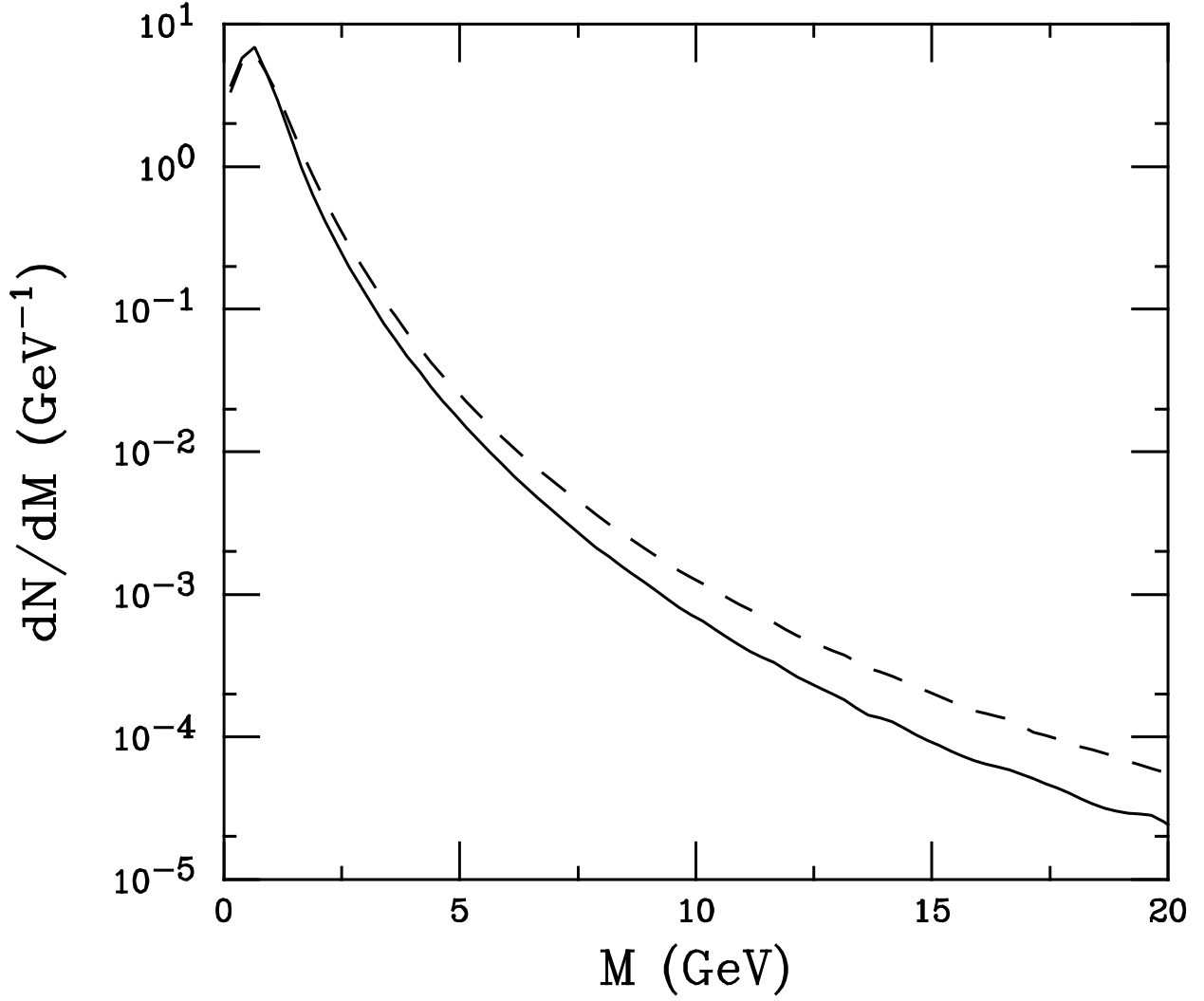


FIG. 3. The invariant mass distribution of lepton pairs from correlated  $D\bar{D}$  decays, integrated over all phase space. The dashed curve is without energy loss, the solid curve includes energy loss with  $dE/dx = -1$  GeV/fm.



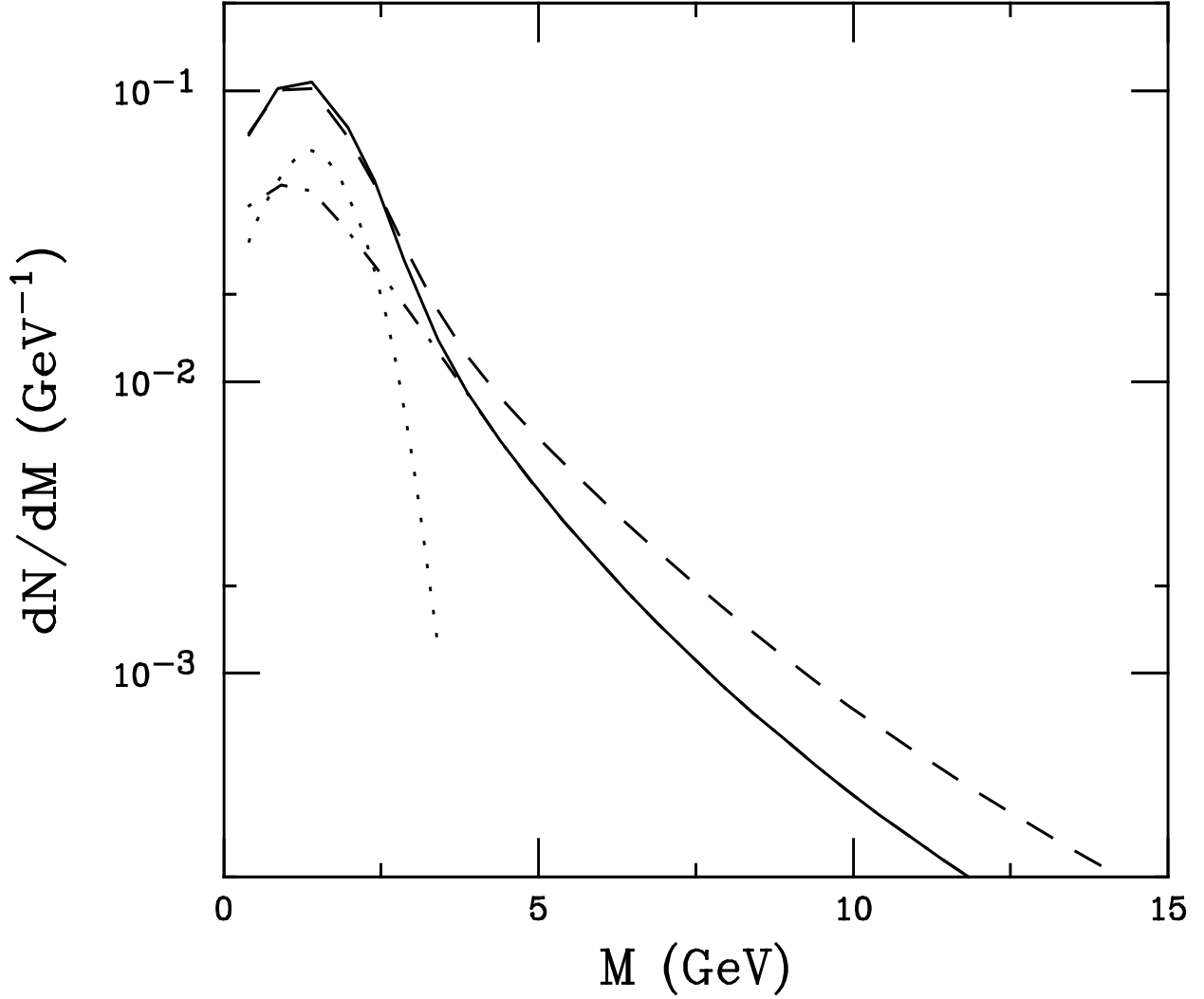


FIG. 4. The invariant mass distribution of lepton pairs from correlated  $B\bar{B}$  decays and single  $B$  decays, integrated over all phase space. The dotted curve is the contribution from semileptonic decay chains of single  $B$  mesons while the dot-dashed curve is from correlated  $B\bar{B}$  decays. Both include energy loss. The dashed curve is without energy loss and the solid curve includes energy loss with  $dE/dx = -1$  GeV/fm. Note that the dashed and solid curves include all single  $B$  and  $B\bar{B}$  pair decays.

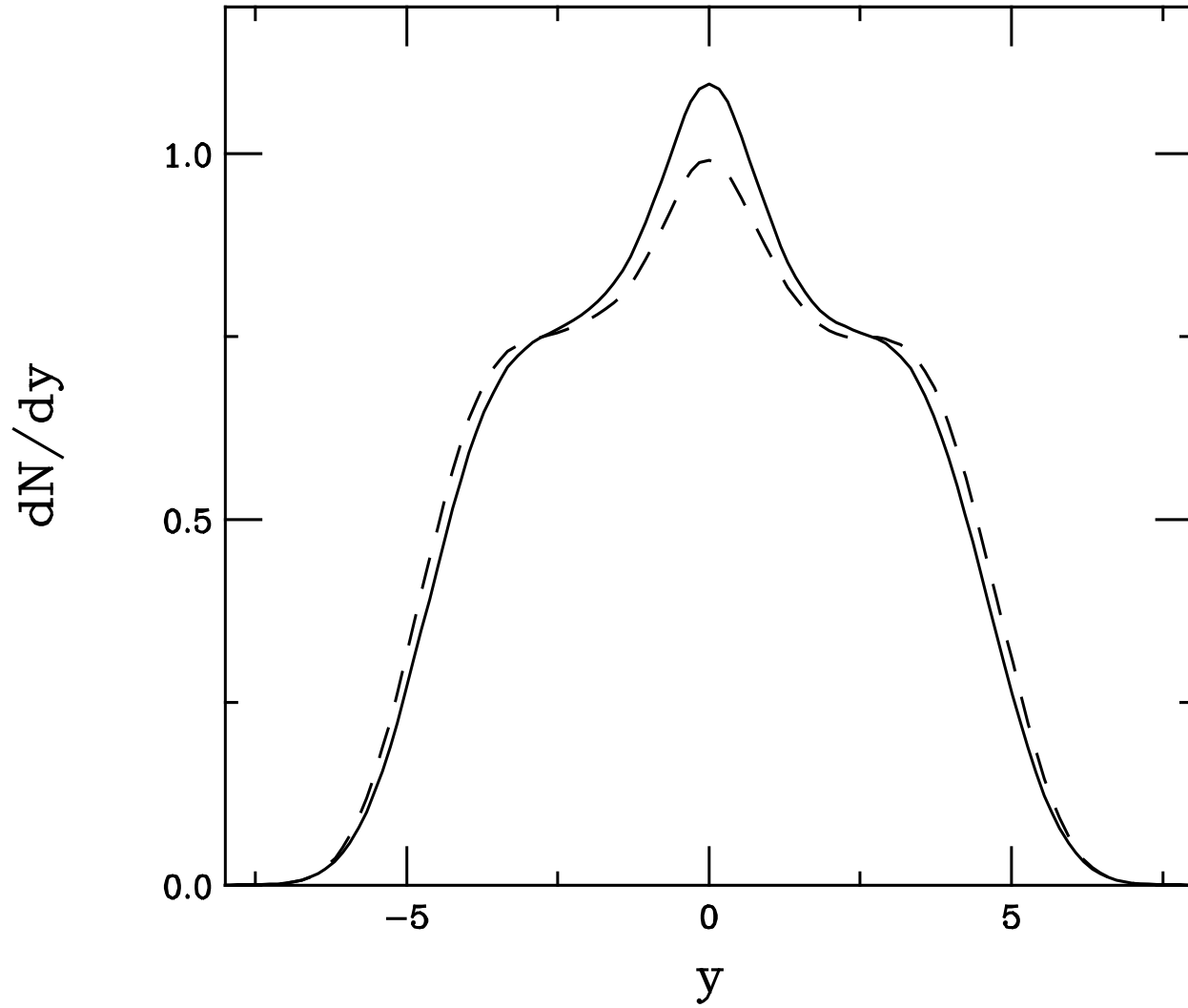


FIG. 5. The rapidity distribution of lepton pairs from correlated  $D\bar{D}$  decays, integrated over all phase space. The dashed curve is without energy loss, the solid curve includes energy loss with  $dE/dx = -1$  GeV/fm.

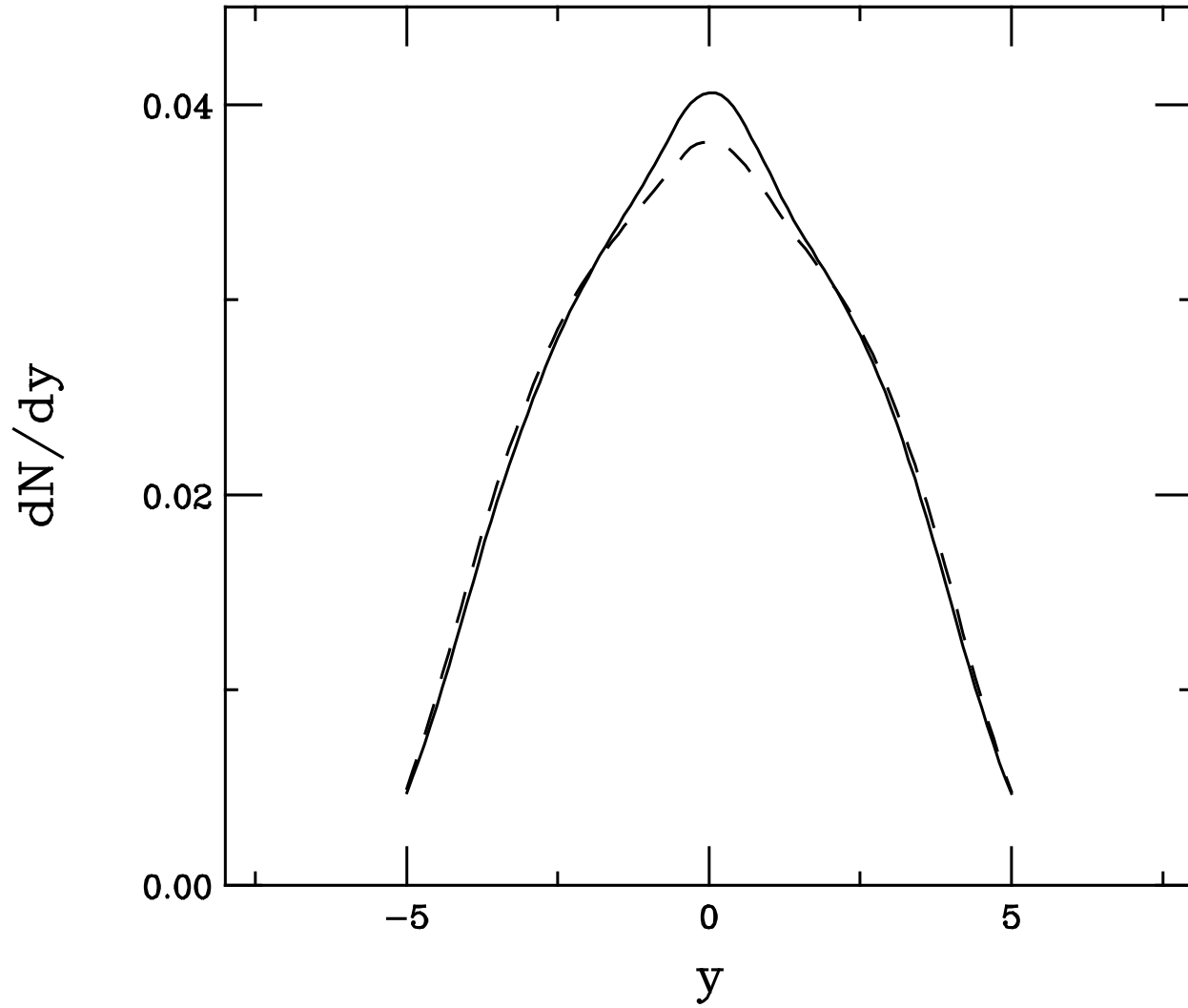


FIG. 6. The rapidity distribution of lepton pairs from correlated  $B\bar{B}$  and single  $B$  decays, integrated over all phase space. The dashed curve is without energy loss, the solid curve includes energy loss with  $dE/dx = -1$  GeV/fm.

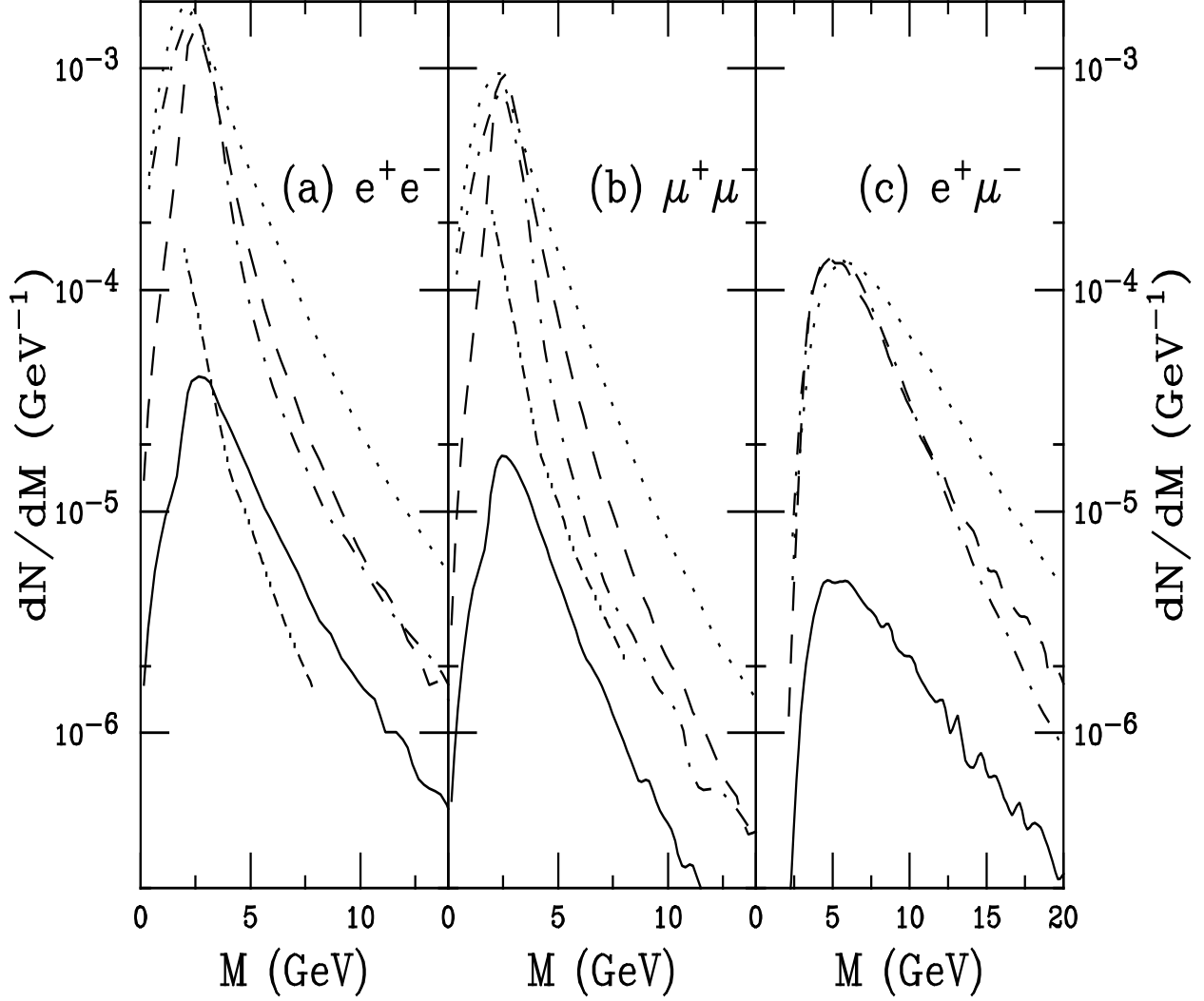


FIG. 7. The dilepton invariant mass distributions in the ALICE acceptance. The  $e^+e^-$  (a),  $\mu^+\mu^-$  (b) and  $e\mu$  (c) channels are shown. The dashed and dotted curves are the  $D\bar{D}$  and summed single  $B$  and  $B\bar{B}$  decays respectively without energy loss. The solid and dot-dashed curves are the corresponding results with  $dE/dx = -1$  GeV/fm. The Drell-Yan rate is given by the dot-dot-dashed curve in (a) and (b).

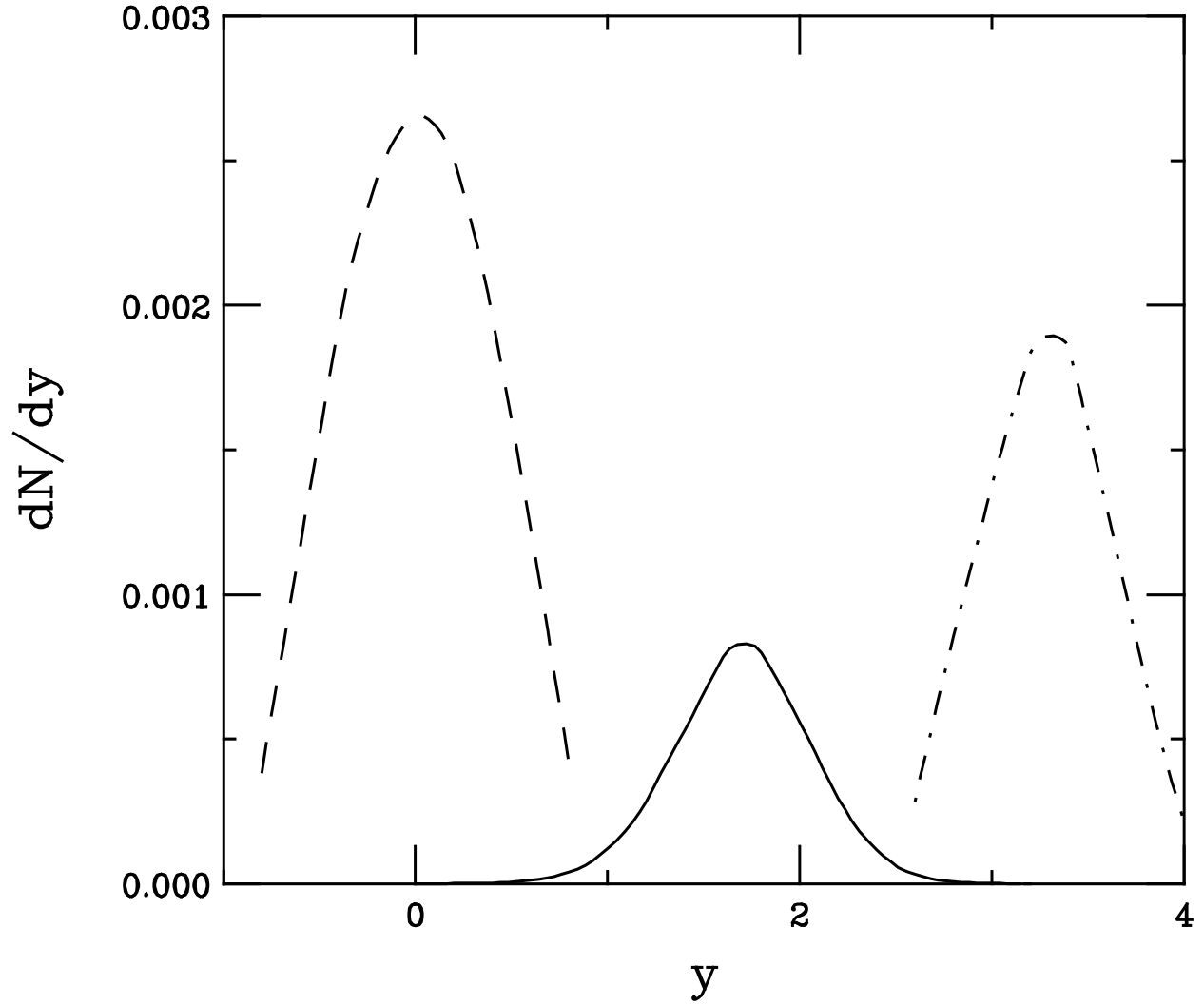


FIG. 8. The rapidity distribution of lepton pairs from correlated  $D\bar{D}$  decays in the ALICE acceptance without energy loss. The  $e^+e^-$  (dashed),  $e\mu$  (solid) and  $\mu^+\mu^-$  (dot-dashed) acceptances are shown.

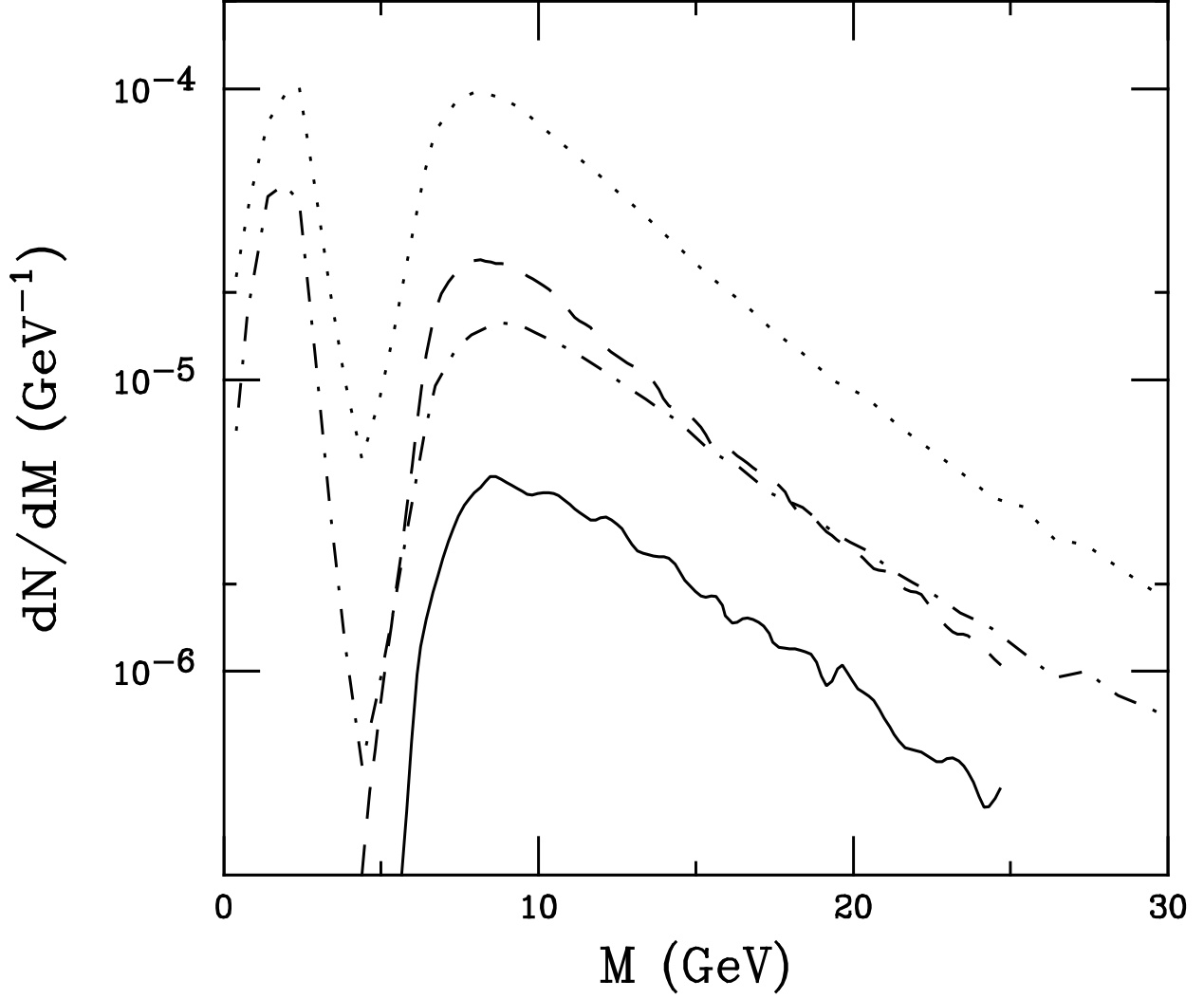


FIG. 9. The dilepton invariant mass distributions in the CMS acceptance. The dashed and dotted curves are the  $D\bar{D}$  and summed single  $B$  and  $B\bar{B}$  decays respectively without energy loss. The solid and dot-dashed curves are the corresponding results with  $dE/dx = -1$  GeV/fm.

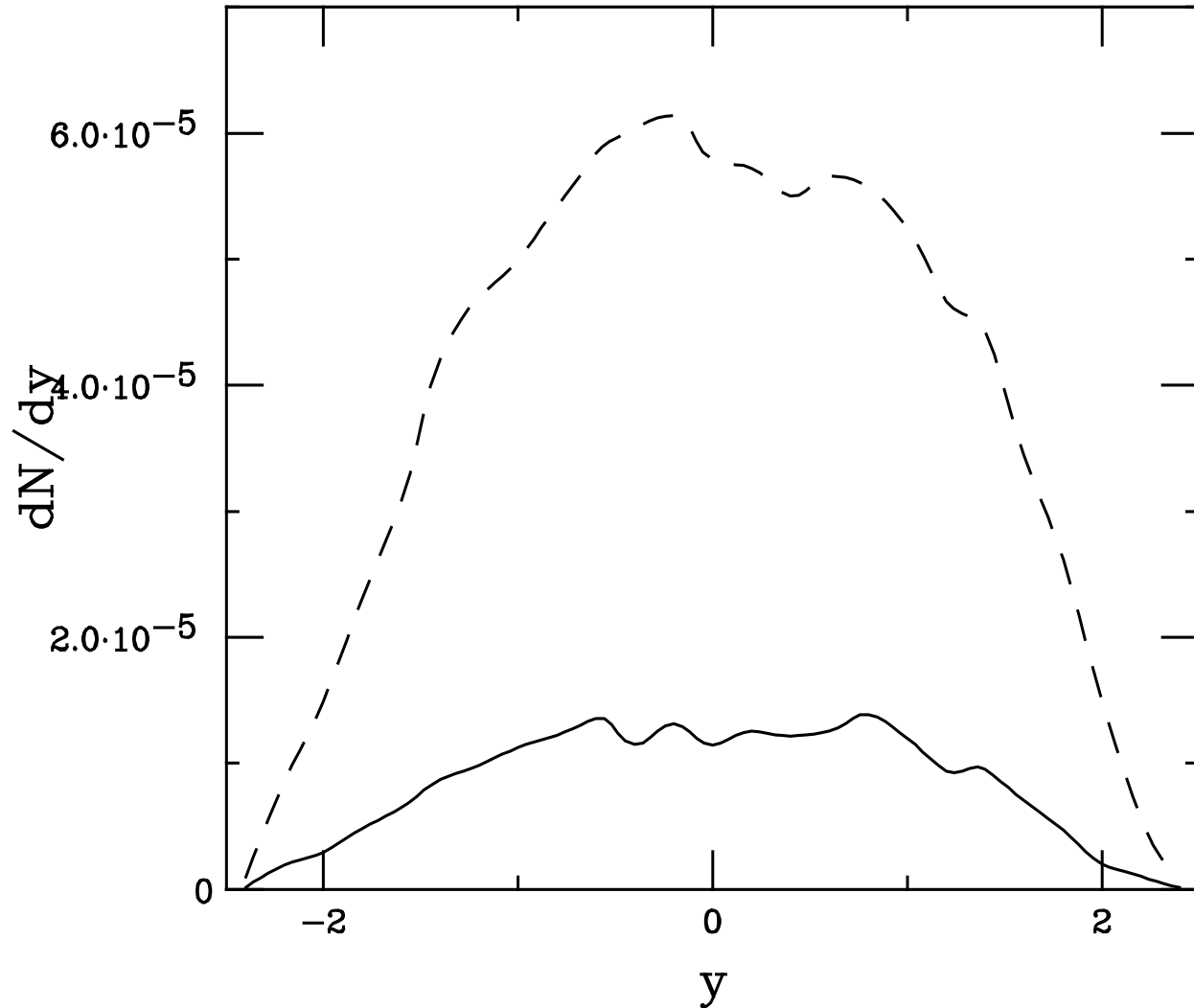


FIG. 10. The rapidity distribution of lepton pairs from correlated  $D\bar{D}$  decays, in the CMS acceptance. The dashed curve is without energy loss, the solid curve includes energy loss with  $dE/dx = -1$  GeV/fm.

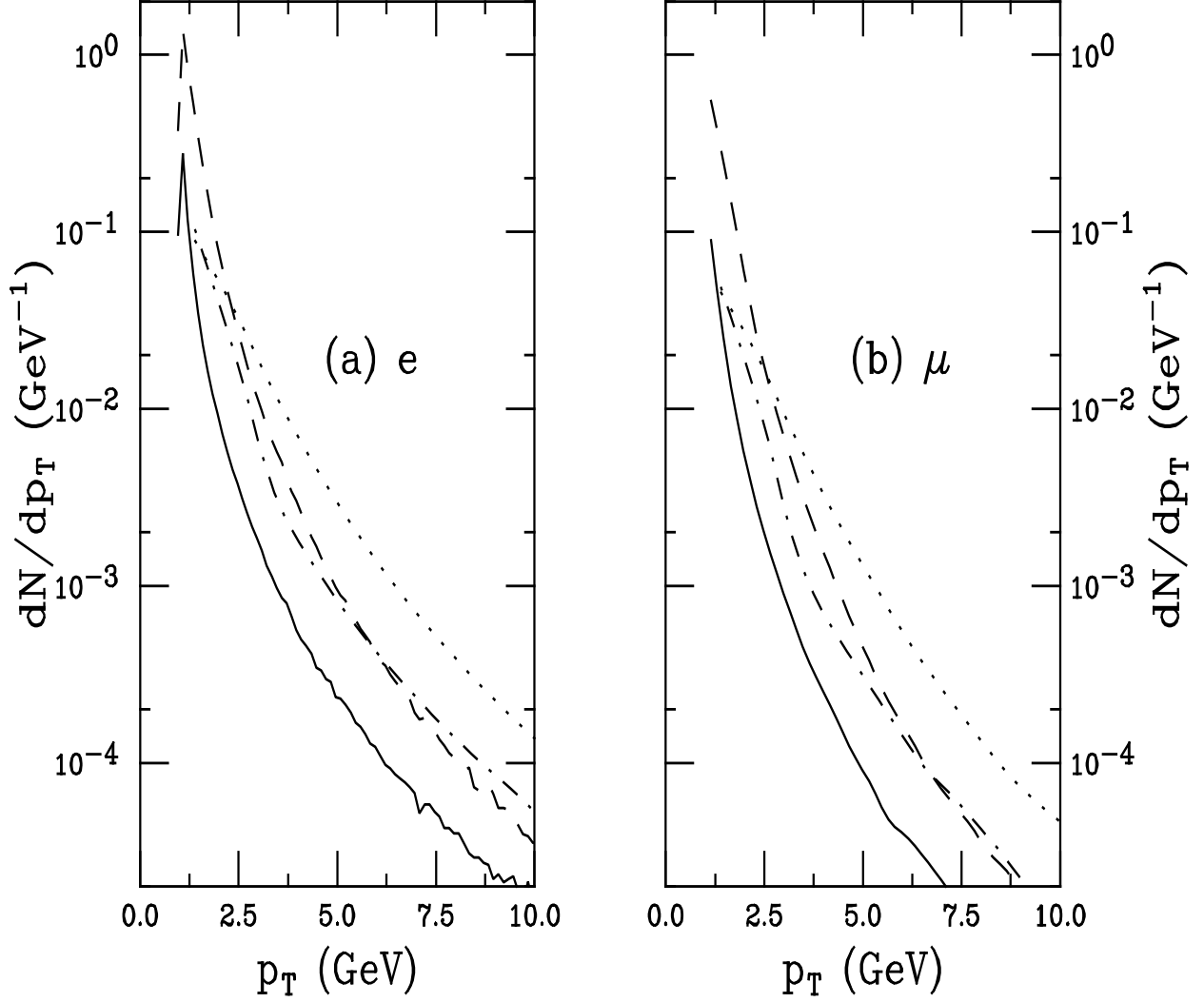


FIG. 11. The  $p_T$  spectrum of single electrons (a) and muons (b) from charm and bottom decays within the ALICE acceptance. The dashed and dotted curves are the  $D$  and  $B$  meson decays respectively without energy loss. The solid and dot-dashed curves are the corresponding results with  $dE/dx = -1$  GeV/fm.



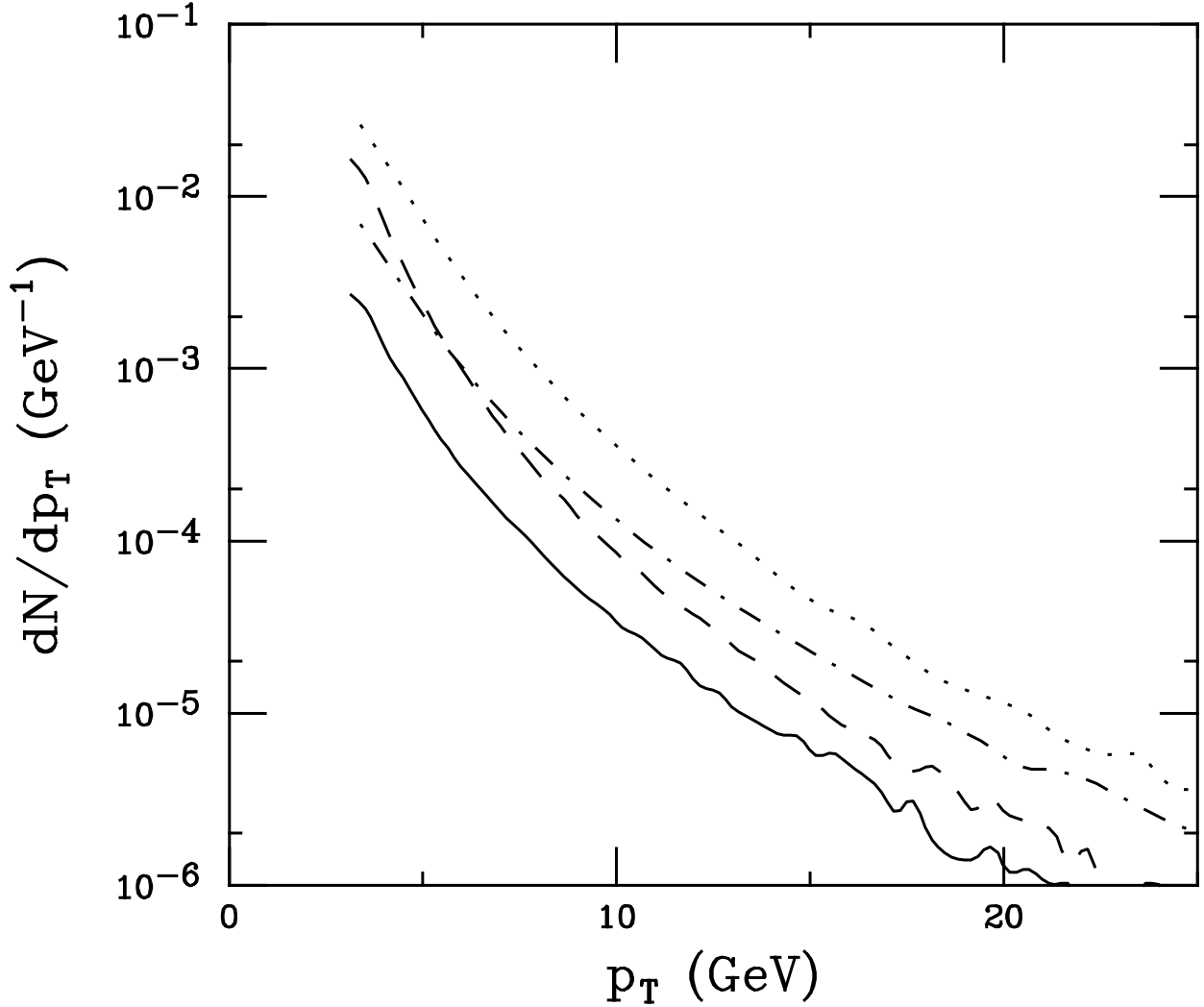


FIG. 12. The  $p_T$  spectrum of single muons from charm and bottom decays within the CMS acceptance. The dashed and dotted curves are the  $D$  and  $B$  meson decays respectively without energy loss. The solid and dot-dashed curves are the corresponding results with  $dE/dx = -1$  GeV/fm.

## REFERENCES

- [1] X.-N. Wang and M. Gyulassy, Phys. Rev. Lett. 68, 1480 (1992).
- [2] E. Braaten and M. Thoma, Phys. Rev. D44, R2625 (1991).
- [3] M. Thoma and M. Gyulassy, Nucl. Phys. B351, 491 (1991); Nucl. Phys. A544, 573c (1992).
- [4] M. Gyulassy and X.-N. Wang, Nucl. Phys. B420, 583 (1994); X.-N. Wang, M. Gyulassy and M. Plumer, Phys. Rev. D51, 3436 (1995).
- [5] R. Baier, Yu.L. Dokshitzer, S. Peigne and D. Schiff, Phys. Lett. B345, 277 (1995).
- [6] R. Baier, Yu.L. Dokshitzer, A.H. Mueller, S. Peigne and D. Schiff, Nucl. Phys. B478, 577 (1996); B483, 291 (1997); B484, 265 (1997).
- [7] M.G. Mustafa, D. Pal, D.K. Srivastava and M.H. Thoma, nucl-th/9711059.
- [8] J.D. Bjorken, Phys. Rev. D27, 140 (1983).
- [9] Z. Lin, R. Vogt and X.-N. Wang, Phys. Rev. C57, 899 (1998).
- [10] T. Sjöstrand, Comput. Phys. Commun. 82, 74 (1994). Further program updates and documentation can be found at <http://www.thep.lu.se/tf2/staff/torbjorn/Pythia.html>.
- [11] A.D. Martin, W.J. Stirling and R.G. Roberts, Phys. Lett. B306, 145 (1993); erratum-ibid. B309, 492 (1993).
- [12] S. Gavin, P.L. McGaughey, P.V. Ruuskanen and R. Vogt, Phys. Rev. C54, 2606 (1996).
- [13] R. Vogt, S. J. Brodsky and P. Hoyer, Nucl. Phys. B383, 643 (1992).
- [14] G.A. Alves *et al.*, (E769 Collab.), Phys. Rev. Lett. 77, 2392 (1996).
- [15] C. Peterson, D. Schlatter, I. Schmitt, and P. Zerwas, Phys. Rev. D27, 105 (1983).
- [16] J. Chirn, in *Proc. Int. Symp. on Production and Decay of Heavy Flavors*, Stanford,

- California, 1987, edited by E. Bloom and A. Fridman, p. 131.
- [17] E.V. Shuryak, Phys. Lett. B78, 150 (1978); Sov. J. Nucl. Phys. 28, 408 (1978).
- [18] D. Fein, Z. Huang, P. Valerio and I. Sarcevic, Phys. Rev. C56, 1637 (1997).
- [19] R.M. Baltrusaitis *et al.*, (Mark-III Collab.), Phys. Rev. Lett. 54, 1976 (1985); erratum-  
ibid. 55, 638 (1985).
- [20] Particle Data Group, R.M. Barnett *et al.*, Phys. Rev. D54, 1 (1996).
- [21] S. Behrends *et al.*, (CLEO Collab.), Phys. Rev. Lett. 59, 407 (1987); B. Barish *et al.*,  
(CLEO Collab.), 76, 1570 (1996).
- [22] ALICE Addendum to the Technical Proposal, CERN/LHCC/96-32 (1996); A. Morsch  
*et al.* (ALICE Collab.), in Proceedings of the 13th International Conference on Ultra-  
Relativistic Nucleus-Nucleus Collisions, Tsukuba, Japan, 1997.
- [23] S. Nagamiya *et al.*, in PHENIX Conceptual Design Report (1993) (unpublished); on  
internet see [http://rsgi01.rhic.bnl.gov/~phenix/phenix\\_home.html](http://rsgi01.rhic.bnl.gov/~phenix/phenix_home.html).
- [24] CMS Technical Proposal, CERN/LHCC 94-38 (1994).
- [25] M. Tannenbaum, Heavy Ion Phys. 4, 139 (1996).